RESEARCH   **Open Access**

Numerical Analysis of the Effect of Afterburning on Damage to the Concrete Structure Under Interior Explosion

Hak Jun Kim[1*], Kyuwan Hwang[1], Yeo Hun Yoon[2] and Hyun-Jin Lee[2]

Abstract

A numerical simulation was performed to analyze how afterburning affects damage to a concrete structure when an explosive detonates inside a room. TNT was used as the explosive for the interior explosion. A reduced scale structure of a Korean apartment room was constructed with reinforced concrete and used as the target room for this research. Interior explosion experiments were performed using TNT 2 kg and TNT 3 kg explosives, to obtain data to verify and calibrate the numerical model. The numerical model was constructed to precisely simulate these interior explosions, especially considering the effect of afterburning, which is a significant phenomenon in enclosed spaces. Numerical simulations were performed with and without the effect of afterburning, and compared with the experiment results. The results showed that the numerical model could well simulate the effects of afterburning in an interior explosion, and that afterburning effects must be considered to more accurately analyze the damage to concrete structures.

Keywords: afterburning, interior explosion, numerical analysis, damage of concrete structure

1 Introduction

Explosions outside buildings have been widely investigated using experimental data, empirical formulas, and numerical analysis techniques, to analyze the pressures and impulses, and the deformation behavior of buildings. On the other hand, reliable research results for explosive detonations inside a building are still lacking, especially numerical simulations that can accurately predict the destructive behavior on the building's walls. This is because, unlike numerical simulations of an external explosion, simulating an interior explosion must also consider various and very complex features of blast wave propagation and energy release in an enclosed space.

When an explosive explodes inside a building, a spherical pressure wave is propagated from the origin of the explosion, meets the wall of the building and is reflected,

and then, as it propagates, is superimposed over the pressure wave that follows it. Unlike external explosions, the temperature inside the building does not rapidly decrease because of the superposing pressure waves and the confined interior space. In such an environment, the reactants in an explosive react with oxygen in the room, releasing energy from combustion. This energy is known as afterburning energy. With TNT, if a temperature greater than the critical temperature at which afterburning can occur is maintained, and a sufficient amount of oxygen is supplied, theoretically an afterburning energy which is 2.23 times greater than the detonation energy can be released (Edri et al., 2012; Schwer, 2016). This can cause more damage to a wall than an external explosion.

If the critical temperature is maintained and sufficient oxygen is supplied, all of the afterburning energy stored in the reactant will be released. However, rooms generally have openings such as windows and doors, and this can lower the interior temperature so that the critical temperature is not maintained long enough to react all of the potential afterburning energy. This makes it impossible

---

Kim *et al. Int J Concr Struct Mater*   (2022) 16:6

Page 2 of 21

to predict the degree of damage to the wall of a building using theories or simple empirical formulas. The effects of the afterburning energy can only be predicted by developing and using a numerical analysis technique that can simulate this phenomenon well.

However, a review of recent studies in the field of interior explosion numerical analysis finds that they are typically limited to studying the behavior of pressure waves and impulses in the explosion chamber, and the study of wall damage remains insufficient. Most of the research that has been conducted so far has experimentally acquired pressure data by assuming that the walls of the chamber or room are not deformed, and then establishing a numerical analysis technique that can simulate this well. (Cao et al., 2014; Edri et al., 2012; Schwer, 2016; Togashi et al., 2010) This is the reason that a precise numerical analysis technique including afterburning phenomena for the entire process, from interior explosion to wall damage, has not yet been established for concrete structures. (Beppu et al., 2010; Esteban & Gebbeken, 2016; Li & Hao, 2014; Li et al., 2012, 2015, 2017; Lia et al., 2015; Mao et al., 2014, 2015; Ngo et al., 2007; Wang et al., 2009; Wu et al., 2009; Xu & Lu, 2006; Yue et al., 2017; Zhang et al., 2015; Zhou et al., 2008).

This study analyzed the effect of afterburning on pressure, impulse, and structural damage following an interior explosion in a Korean apartment room with two openings. The phenomena were analyzed using data from interior explosion experiments and numerical analyses, considering wall damage.

For the interior explosion experiments, reinforced concrete rooms were constructed using the reinforced concrete structure, materials, window/door ratio, and wall connection used in one of the Korean-style apartment rooms. 2 kg and 3 kg of TNT were installed in the center of the room, respectively, as the explosives. During the explosion, the pressures and the displacements of the wall due to the pressures were measured at specific locations. These data were used to confirm the reliability of the numerical analysis results.

For the numerical analyses, the numerical simulation model was constructed considering the various factors to increase the accuracy of the simulation.

2 Interior Explosion Experiment

To verify the numerical simulation results, reinforced concrete rooms were built that mimics one of the scaled-down Korean-style apartment rooms, and interior explosion experiments were performed. The interior volume of the room was 8m^3 (Width × Depth × Height: 2 m × 2 m × 2 m), and the area of the door and window were e 0.9m^2 and 0.3m^2, respectively. Fig. 1 shows the shape of the room. Table 1 provides the detailed specifications of the room.

2 kg and 3 kg of spherical TNT were selected as the explosive for the experiments, and the explosive was placed in the center of the room. Fig. 2 shows the mounted explosive.

In each experiment, the pressure and displacement were measured at the specific location of the wall. As shown in Fig. 3, the four reflect pressure sensors were located on the center of the backside inner wall of the room (inside ❶), the center of the ceiling of the room (inside ❷), the center of the right side inner wall (inside ❸) and the bottom corner of the right side inner wall (inside ❹), respectively, relative to the location of the door. Kulite's PR-type sensors (HEM-375 model) were employed in the experiments. Fig. 4 shows the shape

Fig. 1 Room shape.

Table 1 Room dimensions.

Classification	Dimension
Inner width (mm)	2000
Inner length (mm)	2000
Inner height (mm)	2000
Outer width (mm)	3000
Outer height (mm)	2650
Outer height (mm)	3000
Door width (mm)	600
Door height (mm)	1500
Window width (mm)	600
Window height (mm)	500
wall thickness (mm)	160
Concrete compressive strength (MPa)	31
Maximum aggregate size (mm)	18
Rebar yield strength (MPa)	410
Rebar diameter (mm)	10
Rebar spacing (mm)	150

Fig. 2 Shape of the mounted explosive.

of the sensors installed at the center of the right side (inside ❸) and the bottom corner of the right side (inside ❹).

As shown in Fig. 5, displacement sensors were installed in three places, the center of the backside outer wall of the room, the center of the top side outer wall, and the center of the right side outer wall, relative to the door.

Fig. 6 shows the experimental phenomenon recorded for the 2 kg of TNT, and Figs. 7 and 8 show the pressure and displacement according to time at the measurement positions, respectively.

Fig. 9 shows the experimental phenomenon recorded for the 3 kg of TNT, and Fig. 10 shows the pressure according to time at the measurement positions. Ceiling center pressure and all of the displacements were not measured.

3 Constructing the Simulation Model

In this study, the numerical simulation model was constructed using LS-DYNA™ software. In constructing the simulation model, the Eulerian method was applied to simulate the gas products behavior after explosion. The Lagrangian method was employed to simulate the concrete and reinforcing bars behavior, which were components of the room. The FSI technique was used to simulate the interaction between the gas products generated by the explosion and the concrete wall. To increase the accuracy of the analysis, the simulation model was constructed considering the following factors.

First, when an explosion simulation is performed using a model with a large Eulerian mesh size, the calculated front blast pressure is typically smaller than the actual pressure, because explosive gas and air coexist in the mesh. To compensate for this phenomenon, the behavior of the blast pressure propagation was simulated in the 1D model with small size meshes until just before it contacts the wall, and then all of the pressure value were mapped into the 3D mesh model.

Second, to simulate accurately the degree of damage to the room depending on the amount of explosive, the material model and related parameters of the concrete and reinforcing bars were determined so that the degree of displacement and damage to the concrete wall were close to the experimental data. (Luccioni et al., 2013).

Third, this study analyzed the afterburning energy technique provided by LS-DYNA™ and determined the optimal technique and related parameters, then used them in the simulation.

In addition, among the FSI parameters of LS-DYNA™, the numerical parameters related to pressure transmission and leakage control were determined by comparison with the experimental data, to improve the accuracy of the computational analysis.

3.1 3D Mapping of 1D Analysis Results

The reliable mesh size in the 1D simulation was determined before mapping the 1D explosion simulation results to the 3D Eulerian grid. For several mesh sizes, 1D
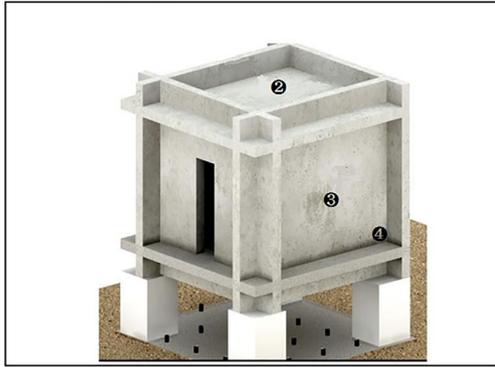
Fig. 3 Reflection pressure sensor locations.
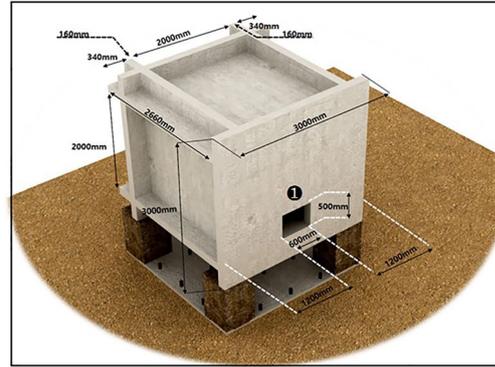
**Fig. 4** Reflective pressure sensor installation shape.

simulations about the explosion of 2 kg and 3 kg of TNT were performed, respectively, and the pressures on the location of 1 m and 1.5 m distance from the detonation position were compared with those calculated by CONWEP code, which is known to be the reliable engineering program to solve the pressure wave propagation due to explosion.

Figs. 11 and 12 show the pressure behavior with time at distances of 1 m and 1.5 m from the initiation position for the 2 kg and 3 kg TNT, respectively. It can be seen that as the mesh size became smaller, from 20 to 5 mm, the pressure behavior was closer to the CONWEP result.

Table 2 summarizes the error between the 1D results and CONWEP results, according to mesh size. Except for the error at the 1.5 m position of 2 kg TNT, the 1D
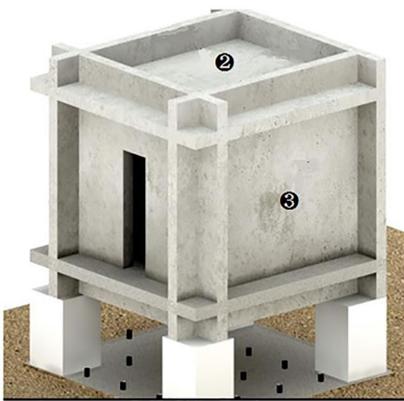
Fig. 5 Displacement sensor positions.

Kim *et al. Int J Concr Struct Mater*   (2022) 16:6

Page 5 of 21
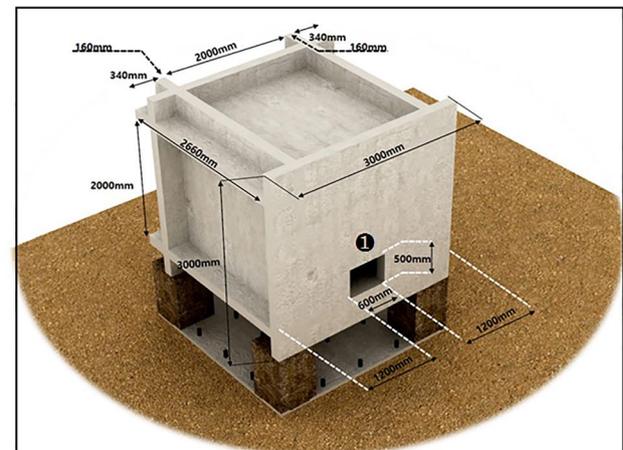
Fig. 6 Interior explosion (TNT 2 kg).

analyses results fell within 5% of the CONWEP result when the mesh size for the 2 kg and 3 kg TNT was 10 mm or less. Based on these results, the mesh size of 5 mm was selected.

In the process of mapping the 1D explosion analyses results to the 3D Eulerian grid, the pressure distribution was checked to determine whether it was well mapped. As shown in Fig. 13, to reflect the same positional conditions of the 1D fluid model in the 3D fluid model space, the pressure results were set 12 positions apart from the detonation point, at regular intervals from 200 to 1000 mm in the horizontal direction, and at 45-degrees in the diagonal direction. The reliability of the ALE Mapping method was reviewed by comparing the pressure results with the 1D fluid model results.
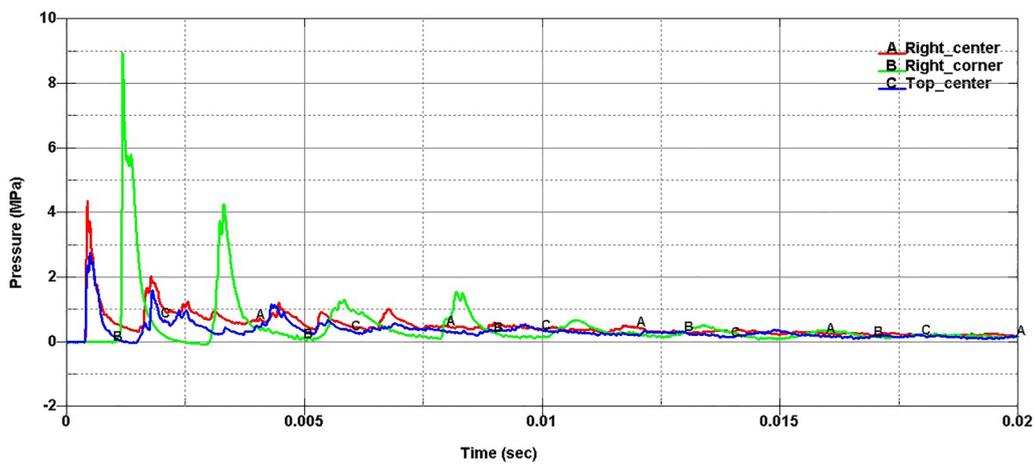
Fig. 7 Pressure measurement data (TNT 2 kg).
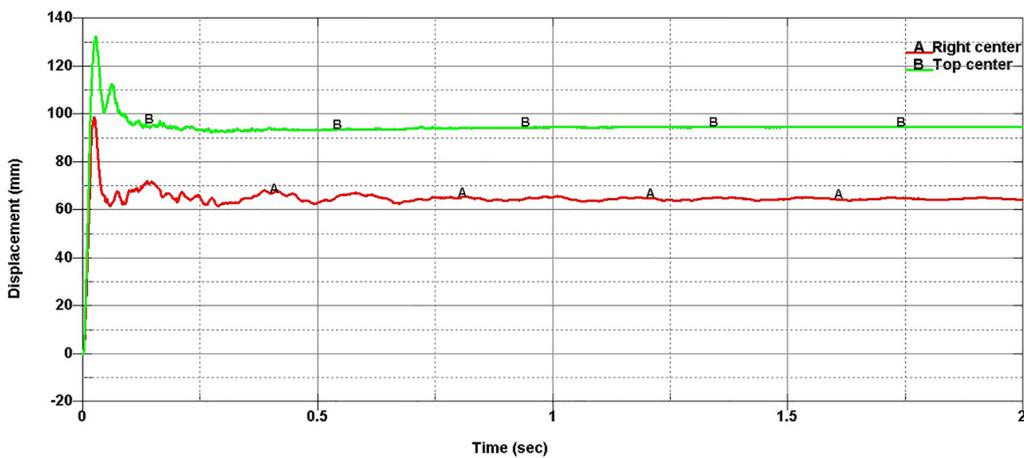
Fig. 8 Displacement measurement data (TNT 2 kg).

Fig. 9 Interior explosion (TNT 3 kg).

Fig. 14 compares the results of the 1D model and the 3D model in the horizontal and diagonal directions, 45 degrees from the detonation point. Although a slight error occurred at a distance of 945 mm, it was confirmed that the 1D fluid model analyses results were applied well as the initial condition of the 3D fluid model at 0.4 ms.

3.2 Construction of the Reinforced Concrete Room Structural Model and Physical Property Model

The room structure model used for the analysis was a reinforced concrete room with a front door (0.4 m × 1.5 m) and a rear door (0.6 m × 0.5 m) and an internal volume of 2 m × 2 m × 2 m (Width × Depth × Height) as in the experimental specifications. HD10 reinforcing bars were inserted inside the concrete wall in the form of double reinforcement with a covering thickness of 40 mm and intervals of 150 mm. Figs. 15 and 16 show the shape of the room and the shape of the internal reinforcements, respectively.

The concrete was modeled as a 3D element surrounding the rebar structure, and the reinforcing bar was modeled as a 1D element. A total of 115,080 3D elements and 32,152 1D elements were modeled. Fig. 17 shows the element model of the reinforced concrete room.

A 6-DOF fixed boundary condition was applied using the nodes at the four bottom points, as shown in Fig. 18, to support the structure, such as the experimental condition.

The concrete used for the experiment and analysis had a compressive strength of 31 MPa, and the material model used for the concrete was the MAT_CONCRETE_DAMAGE_REL3 property model (Schwer & Malvar, 2005) in the LS-DYNA™ material model library. This material model can take into account strain, strain rate, damage and DIF. We also used maximum principal strain as the erosion criteria of the concrete.

The MAT_Piecewise_Linear_Plasticity material model in the LS-DYNA™ material property model library was used for the reinforcing bars. Their diameter was 9.53 mm and yield strength was 400 MPa.

The contact between the reinforcing bars and the concrete was considered using the CONSTRAINED_BEAM_IN_SOLID keyword of LS-DYNA™.

3.3 Establishing the Afterburning Simulation Model

With TNT, if the ambient temperature is maintained above 900 K after an explosion, afterburning energy is released by the reactions of the generated gas. To simulate this phenomenon, the modified JWL equation of state was used which the afterburning energy term was added to, as shown in Eq. 1. For the afterburning energy value, the Q of TNT, the explosive used in this study, the theoretical energy value (10.01 MJ/kg) released by the oxidation of the reactants generated by the explosion was used (Schwer, 2016):
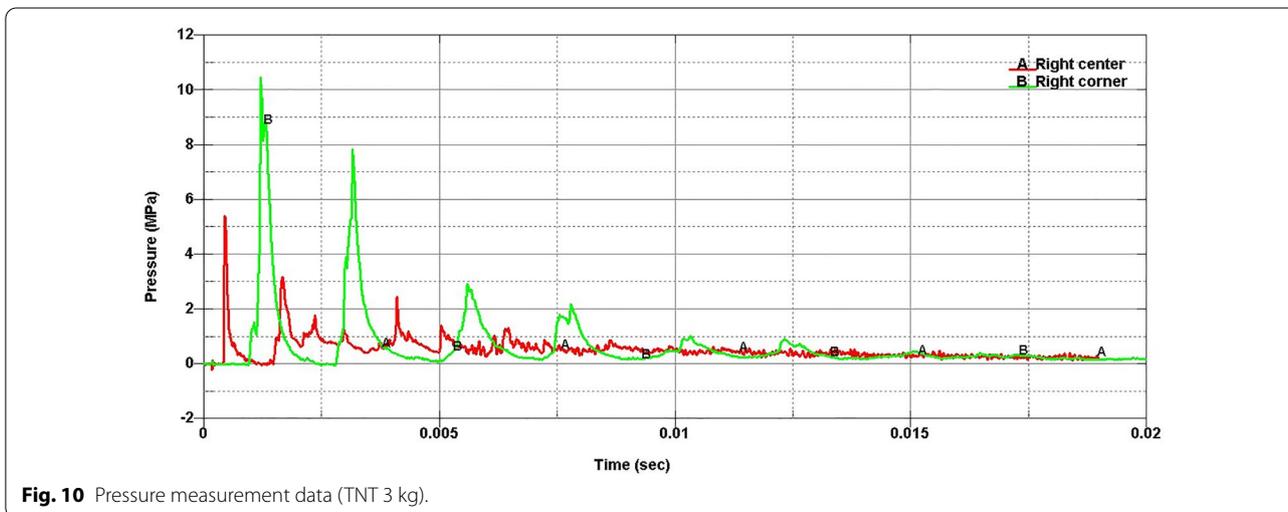

Fig. 10 Pressure measurement data (TNT 3 kg).
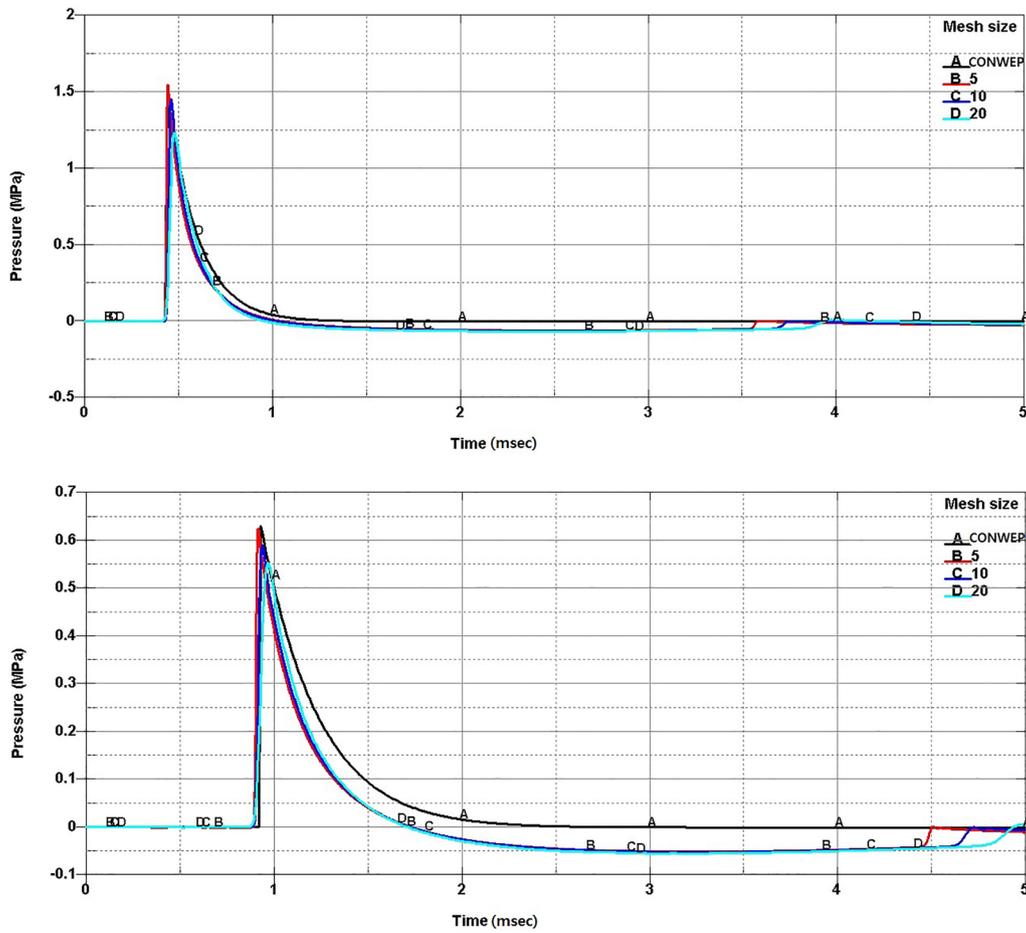
Fig. 11 Pressure behavior with time at distances of 1 m (top) and 1.5 m (bottom) from the 2 kg TNT detonation position.

$$P = A\left(\frac{\omega}{R_1 V}\right)e^{-R_1 V} + B\left(\frac{\omega}{R_2 V}\right)e^{-R_2 V} + \frac{\omega(E + \mathbf{Q})}{V},$$

(1)

where P is the pressure, V is the specific volume, E is the interior energy, A, B, R1, and R2, and ω is the parameters of JWL equation of state.

In the analysis, it is necessary to determine the afterburning start time and end time. For TNT the interior temperature must be maintained at 900 K or higher for afterburning to occur inside the room, as mentioned above. Therefore, in this study, the afterburning start time was determined as the time when the interior temperature reached 900 K, and the end time was determined to be the time when the interior temperature then dropped below 900 K.

The LS-DYNA™ analysis code does not produce temperature as the analysis result. However, since it produces the interior energy according to time, the

relationship between the interior energy and temperature in the ideal gas equation of state (Eq. 2) was used to determine the afterburning start and end times. (Schwer, 2016) In the explosions of 2 kg and 3 kg of TNT, the interior energy at an interior temperature of 900 K was calculated to be $1.501E + 09$ J and $2.225E + 09$ J, respectively:

$$E = T \times C_v,$$

(2)

where E is the interior energy, T is the temperature C_V is the heat capacity.

Figs. 19 and 20 show the afterburning start time and end time, determined using the calculated interior energy. For the 2 kg TNT, the afterburning start time and end time were determined to be 1.15 ms and 9.36 ms, respectively, and for the 3 kg TNT, 0.76 ms and 10.5 ms were determined.

Kim *et al. Int J Concr Struct Mater*   (2022) 16:6

Page 8 of 21
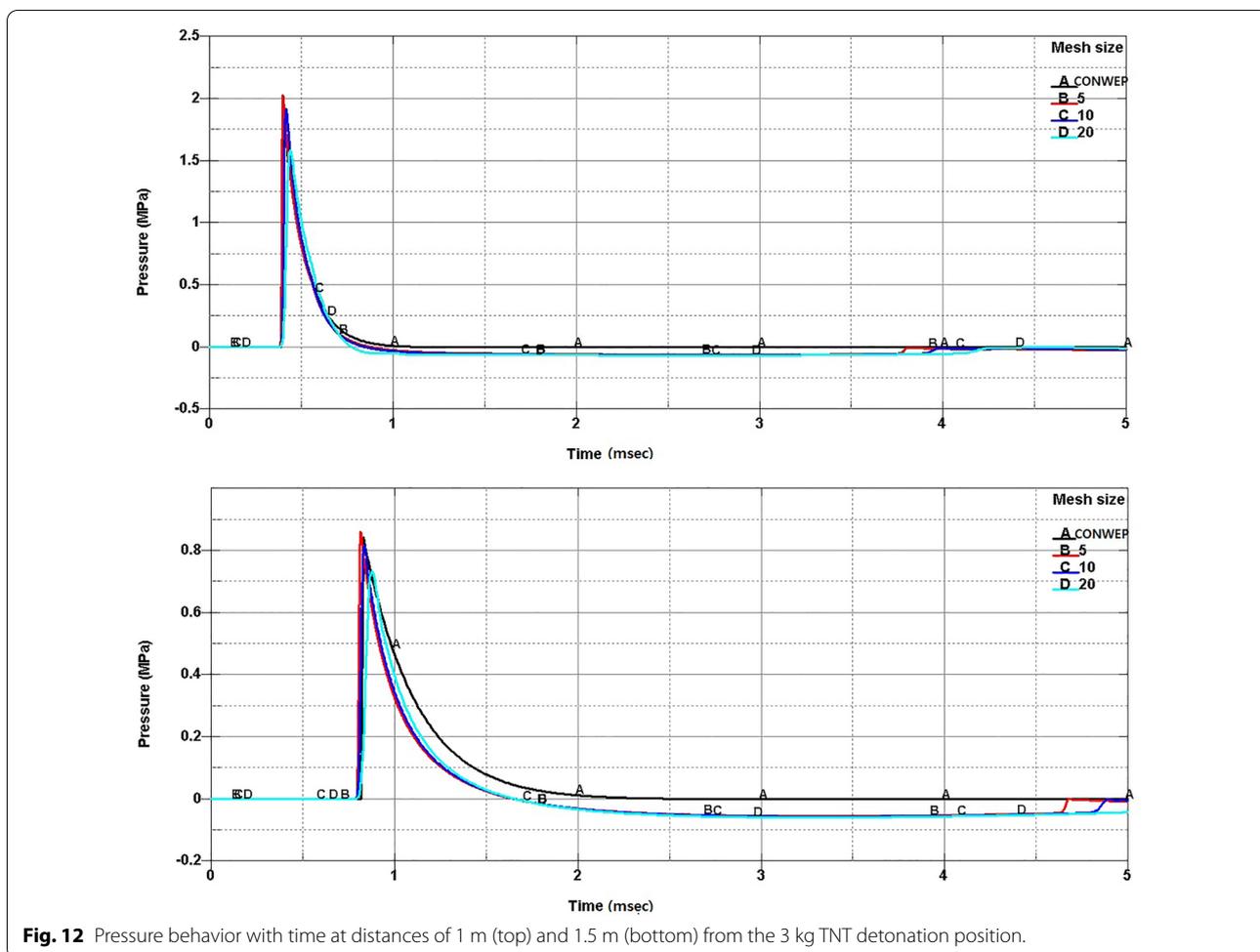
Fig. 12 Pressure behavior with time at distances of 1 m (top) and 1.5 m (bottom) from the 3 kg TNT detonation position.

Table 2 2 kg and 3 kg TNT pressure comparison.

TNT (kg)	Analysis model	mesh size (mm)	Distance (m)	Peak pressure (MPa)	Error (%)
2.0	CONWEP	–	1.0	1.522	–
			1.5	0.630	–
	1D model	20	1.0	1.234	23.34
			1.5	0.553	13.92
		10	1.0	1.454	4.68
			1.5	0.591	6.60
		5	1.0	1.545	1.49
			1.5	0.625	0.80
3.0	CONWEP	–	1.0	1.928	–
			1.5	0.843	–
	1D model	20	1.0	1.584	21.72
			1.5	0.734	14.85
		10	1.0	1.915	0.68
			1.5	0.815	3.44
		5	1.0	2.027	4.88
			1.5	0.861	2.09

4 Numerical Analysis Results of Afterburning Effect

4.1 TNT 2 kg Numerical Analysis Results

To analyze the effect of afterburning, the simulation results with afterburning and without afterburning were compared with the experimental results for the interior explosion of 2 kg of TNT. Figs. 21 and 22 compare the two calculation results with the experimental results for pressure and impulse changes over time at the center of the right side inner wall (named to "right center"), and the bottom corner of the right side inner wall (named to "right corner"), relative to the door in the room. Table 3 compares the peak pressure and impulse values.

Comparing the pressure changes over time, with the first peak pressure generated by the reflection of the blast wave from the wall, the simulation result with afterburning was the same as the result without afterburning. However, for the other peak pressures the results with afterburning were calculated to be larger than the results without it. For this reason, the impulse acting on

Kim *et al. Int J Concr Struct Mater* (2022) 16:6

Page 9 of 21
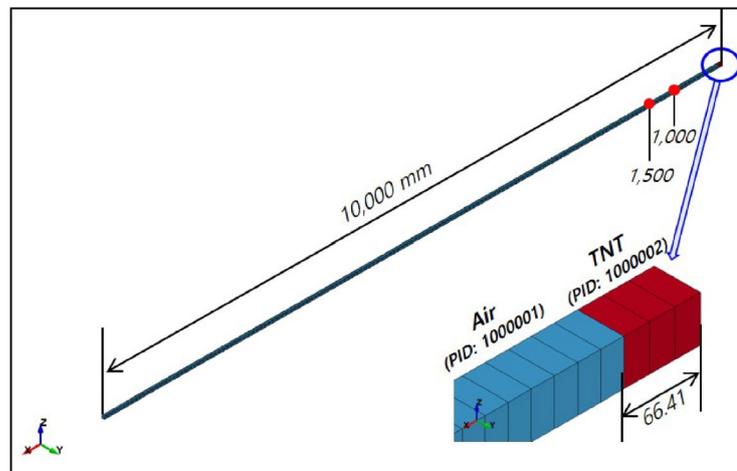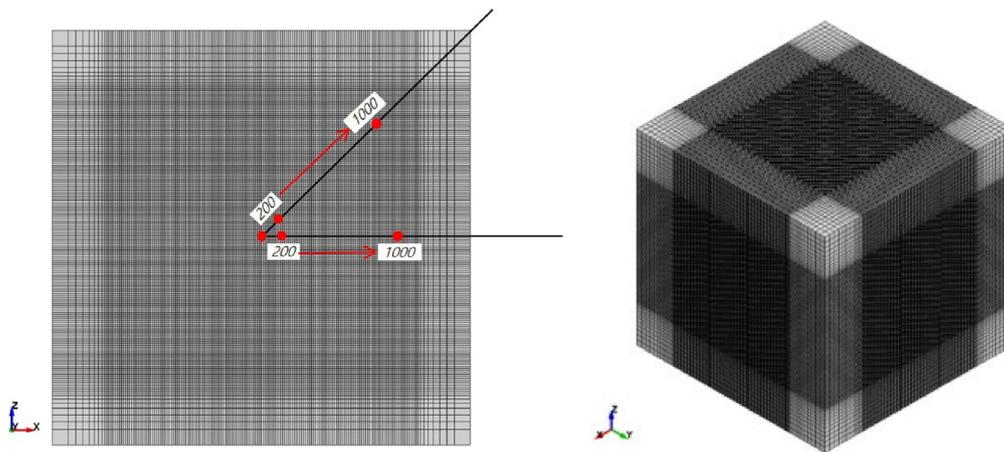
(a) 1D ALE model

(b) 3D ALE model

Fig. 13 ALE mapping reliability review model.

the deformation of the structure was also calculated to be larger when afterburning was applied.

Compared with the experimental data, the error was smaller when afterburning was applied than when not applying it. The quantitative comparison of the experimental results with the simulated results with afterburning showed that, with respect to pressure, the errors for the simulated first, second, and third peak pressures at "right center" were − 11.9%, 15.5%, and − 25.3%, respectively. The impulse on "right center" was − 14.1%, indicating a reliable result.

For "right corner", the errors of the simulated first, second, and third peak pressures were 4.2%, − 7.9%, and 28.2%, respectively. The impulse on "right corner" was − 9.2%, indicating a reliable result.

Fig. 23 compares the shape of the damaged structure after the explosion for the two calculations and experiments. Fig. 24 compares the two calculated results with the experimental results for the change in displacement with time at the center of the top side outer wall (named "top center") and the center of the right side outer wall (named "right center") relative to the door,
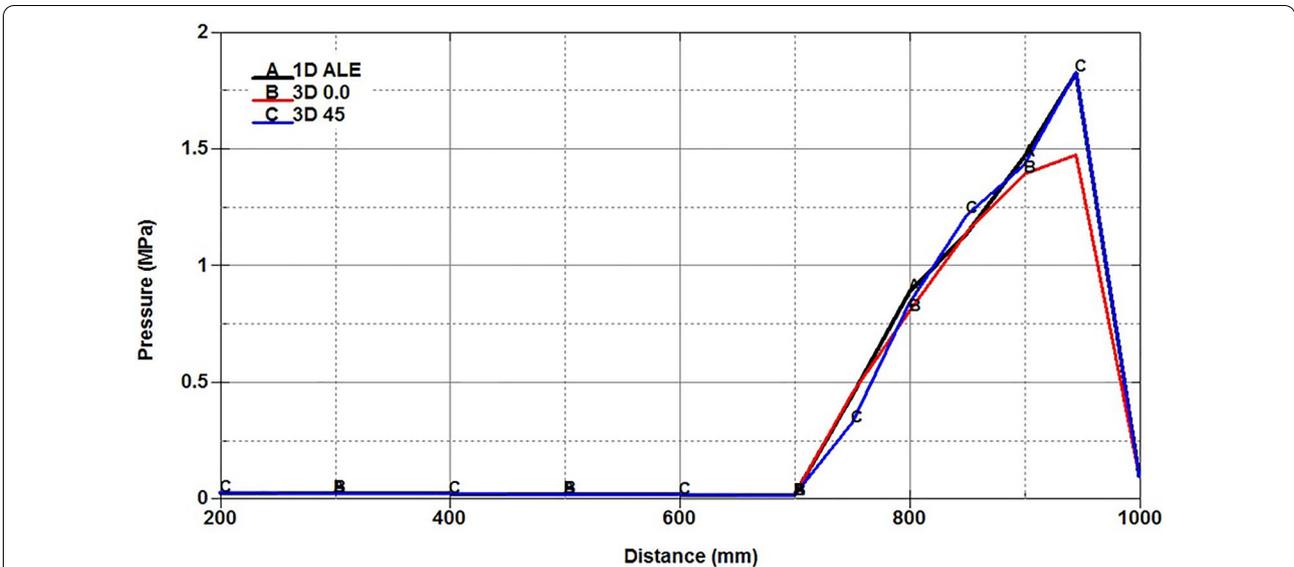
Fig. 14 ALE mapping reliability review analysis result (pressure comparison).
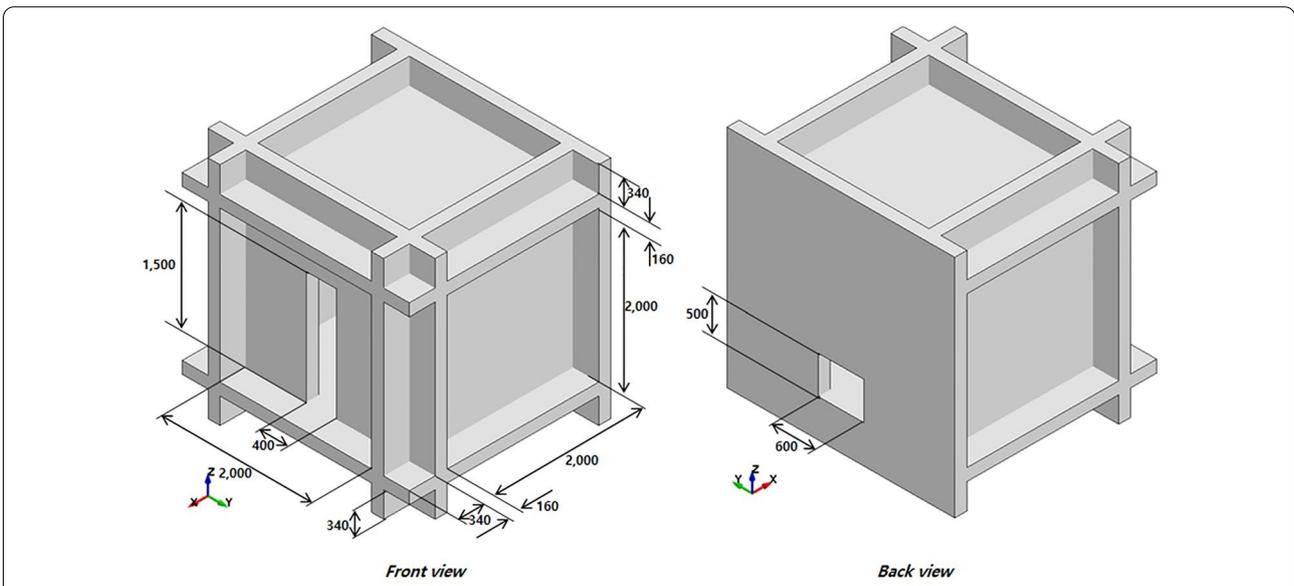
Fig. 15 Reinforced concrete room shape.

and Table 4 compares the maximum displacement and final displacement.

Comparing the displacement with and without the afterburning condition, the results when applying the afterburning condition were closer to the experimental value, with errors of -17.3% and 9.1%, respectively, in the maximum displacement and final displacement at "top center". In the case of "right center", applying the afterburning condition resulted in an error of -1.0% and 22.5% in the maximum displacement and the final

displacement, respectively, which was closer to the experimental values.

4.2 TNT 3 kg Numerical Analysis Results

Next, the results of the numerical simulation with afterburning applied and not applied were compared for the interior explosion of the 3 kg explosive. Fig. 25 shows the results of the shape of the structure damage after the explosion, both calculated and experimental. Figs. 26 and 27 compare the two calculated results with the
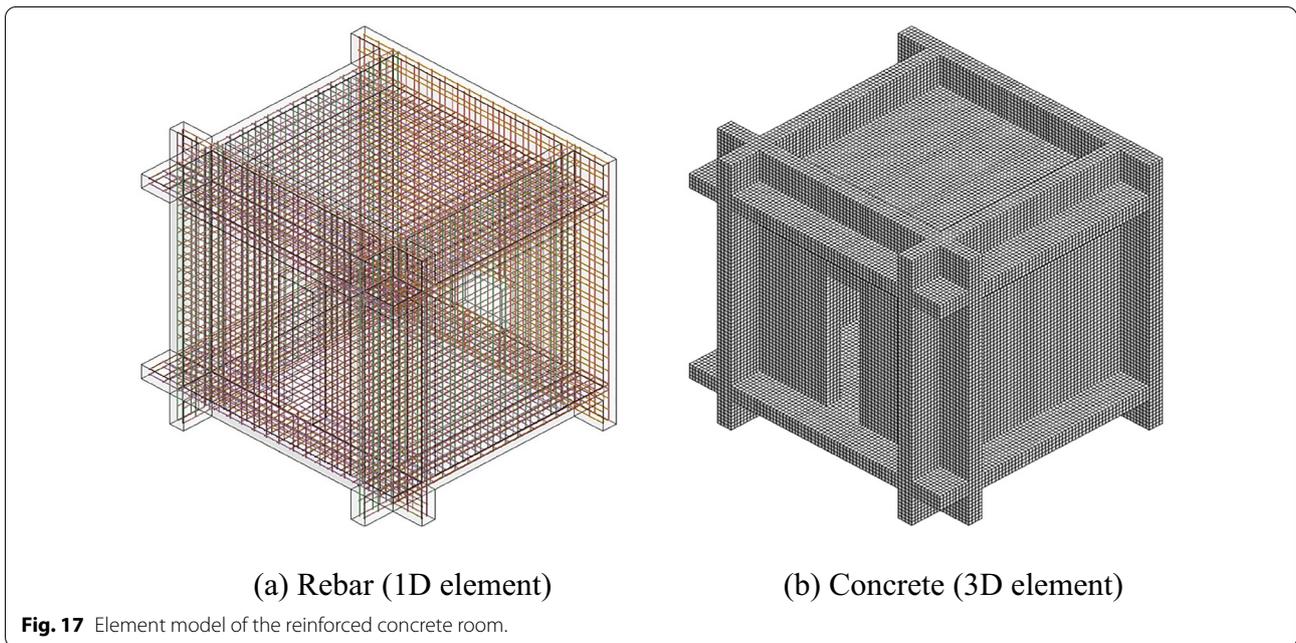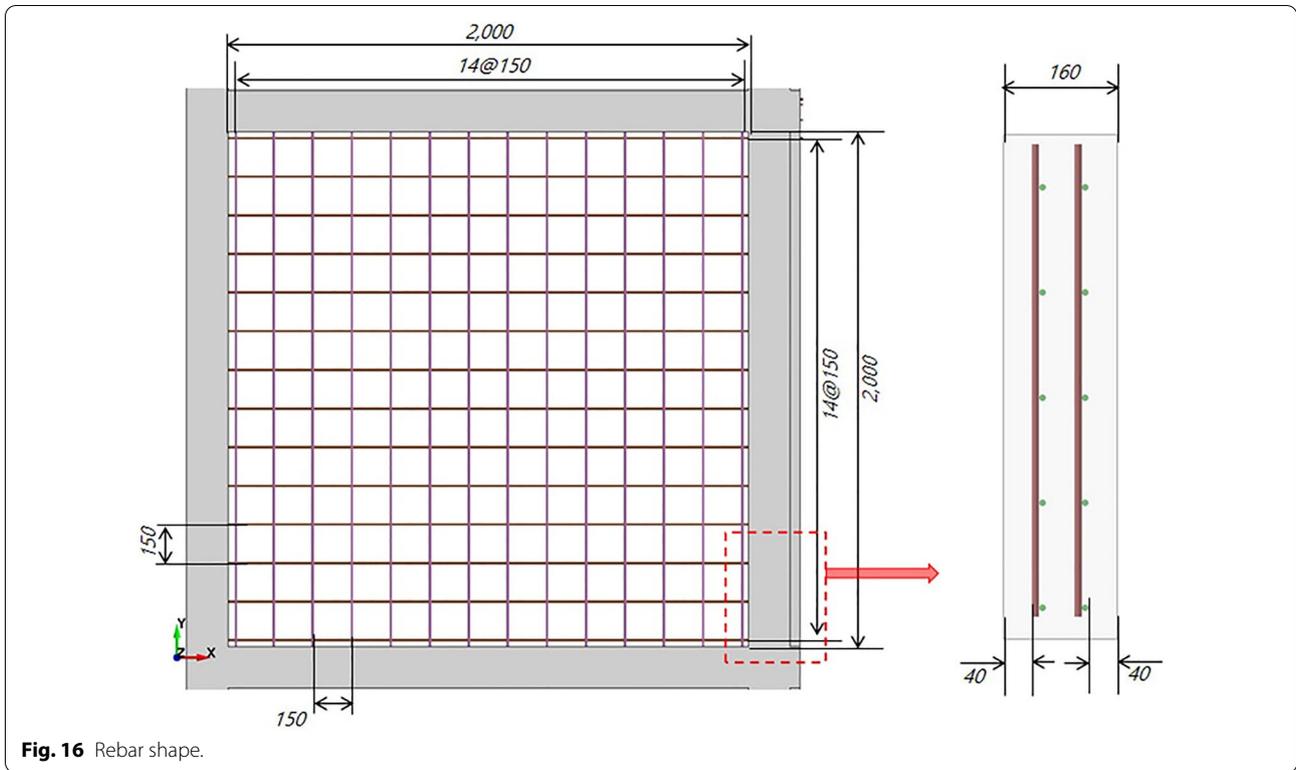
Fig. 16 Rebar shape.

(a) Rebar (1D element)   (b) Concrete (3D element)

Fig. 17 Element model of the reinforced concrete room.

experimental results for pressure and impulse changes over time at the center of the right side inner wall (named to "right center") and the bottom corner of the right side inner wall(named to "right corner"), relative to the door

in the room. Table 5 compares the peak pressure and impulse values.

Comparing the pressure changes over time, as in the 2 kg result, for the first peak pressure generated by the
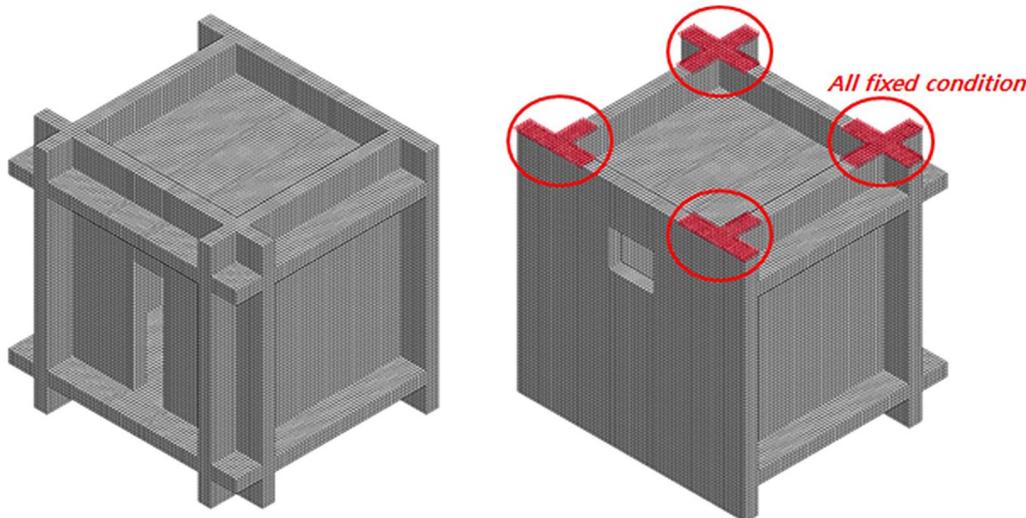
Fig. 18 Boundary condition of the reinforced concrete room.
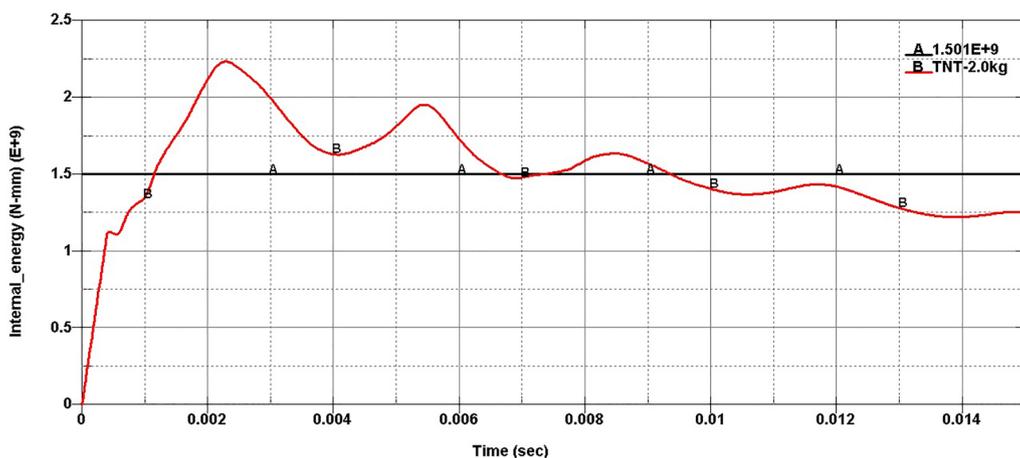
Fig. 19 TNT 2 kg afterburning start time and end time.

reflection of the blast wave from the wall, the simulation result with afterburning was the same as the result without afterburning, but for the other peak pressures, the results with afterburning were calculated to be larger than the results without it. For this reason, the impulse acting on the deformation of the structure was also calculated to be larger when afterburning was applied.

The errors compared with the experimental results were smaller with afterburning than without it, and the errors were smaller than in the case of 2 kg.

The quantitative comparison of the results of afterburning with the experimental results showed that, in the case of pressure, the errors of the simulated first, second,

and third peak pressures at the center of "right center" were 18.8%, 5.6%, and − 32.1%, respectively. The impulse on "right center" was 3.7%, indicating a reliable result.

For "right corner", the errors of the simulated first, second and third peak pressures from the experiment were 41.5%, − 34.4%, and − 37.0%, respectively. The error was large, but the impulse error related to the destruction of the wall was -0.6%, indicating a reliable result.

Fig. 28 and Table 6 compare the displacements with time for the two calculations at the center of the top side outer wall (named "top center") and the center of the right side outer wall (named "right center") relative to the door of the room. Displacement data could not

Fig. 20 TNT 3 kg afterburning start time and end time.

(a) Right center

(b) Right corner

Fig. 21 Pressure comparison over time.
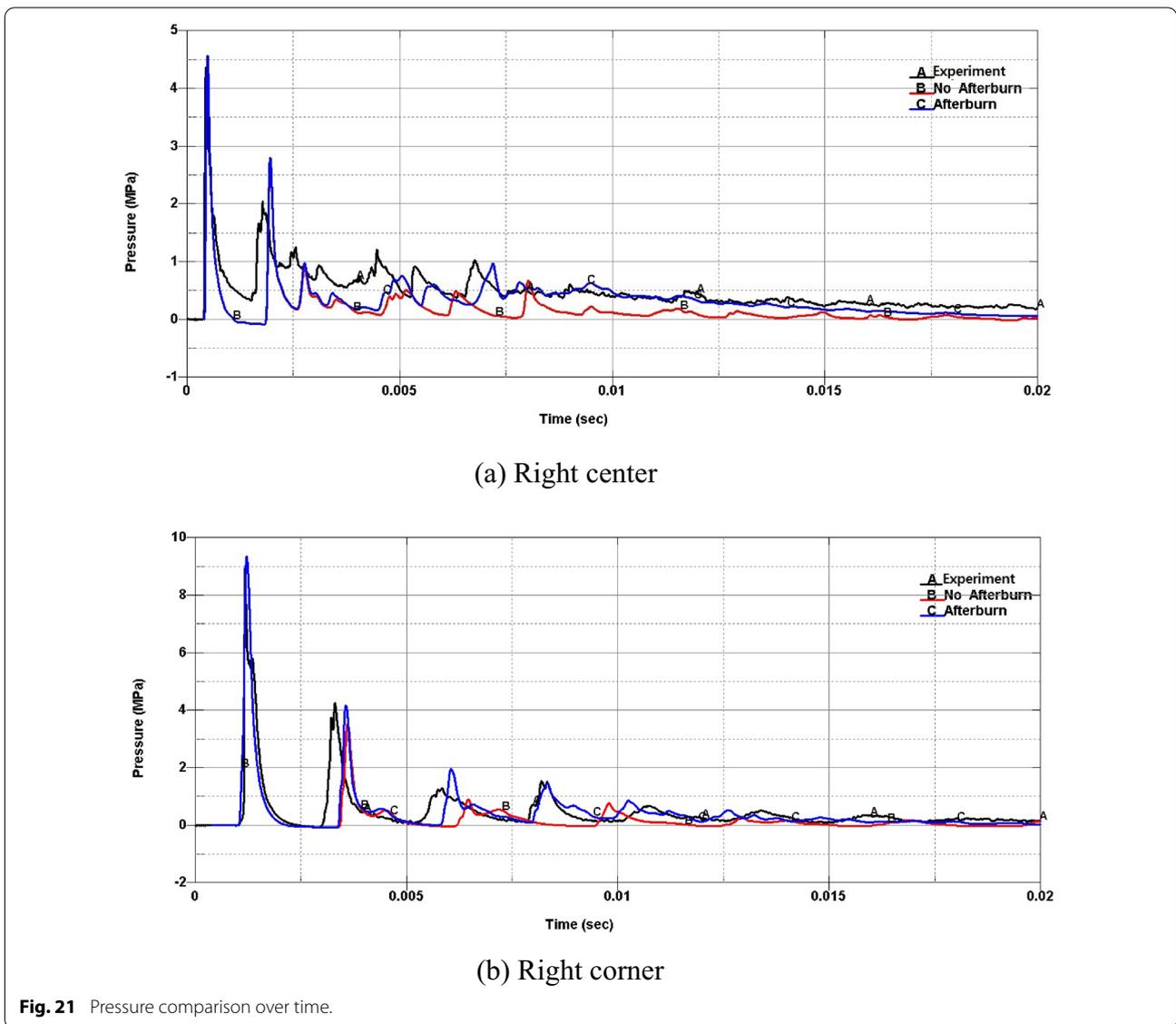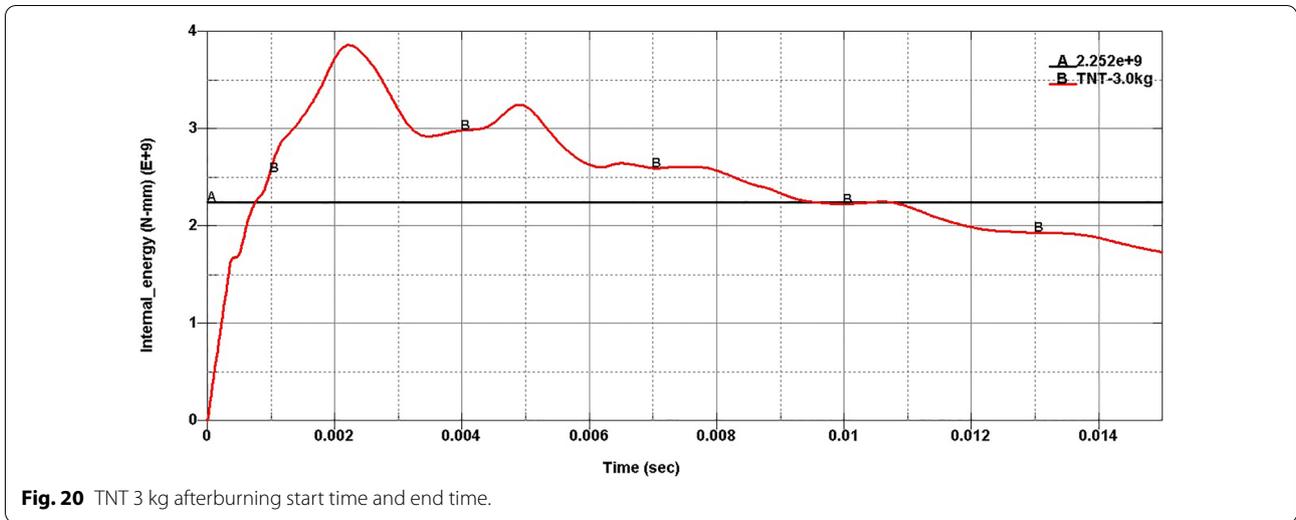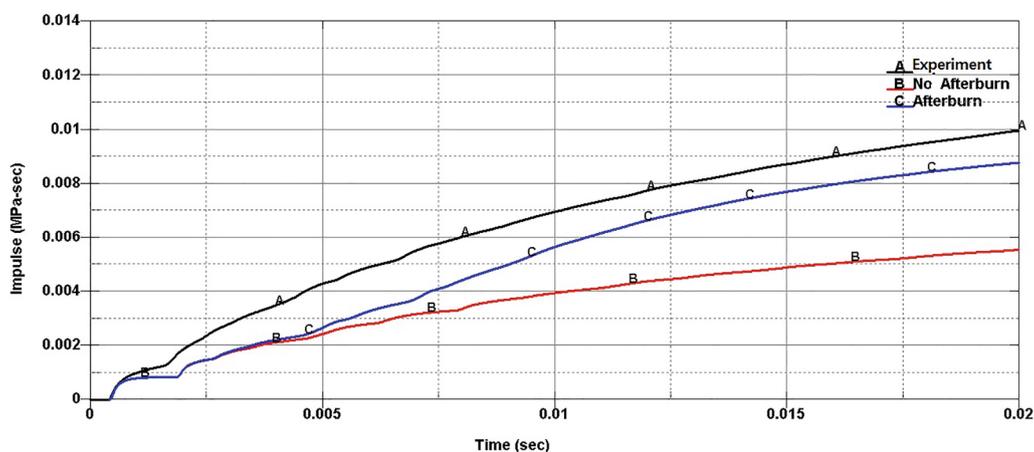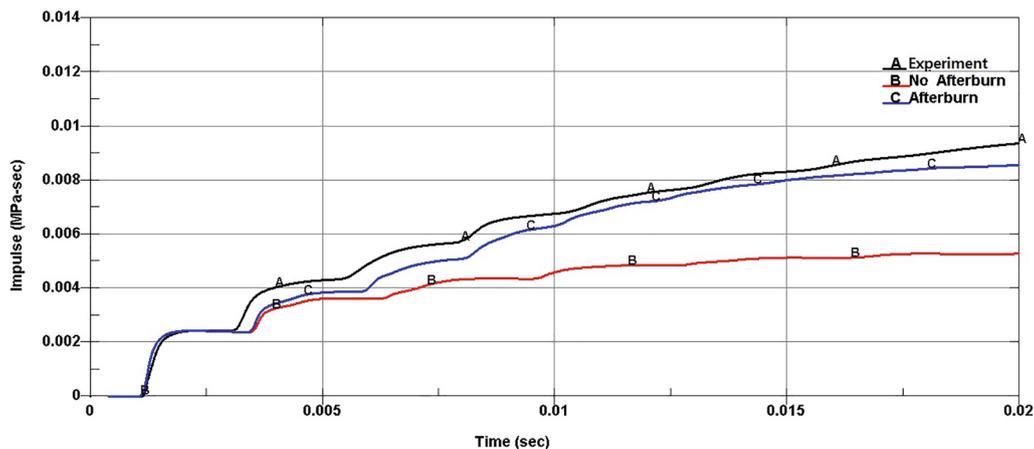
(a) Right center

(b) Right corner

Fig. 22 Impulse comparison over Time.

Table 3 Comparison of peak pressure and impulse.

Position (TNT: 2 kg)		Peak pressure (MPa)						Impulse (MPa-msec)	
		1st	Error (%)	2nd	Error (%)	3rd	Error (%)	–	Error (%)
Experiment	Right center	4.362	–	2.047	–	1.216	–	9.963	–
	Right corner	8.948	–	4.283	–	1.307	–	9.369	–
No Afterburn	Right center	4.567	− 11.9	2.787	− 16.0	0.894	− 31.8	3.591	− 45.7
	Right corner	9.350	4.2	3.530	− 22.1	0.906	− 40.8	5.291	− 44.0
Afterburn	Right center	4.567	− 11.9	2.801	15.5	0.980	− 25.3	6.819	− 14.1
	Right corner	9.352	4.2	4.174	− 7.9	1.962	28.2	8.577	− 9.2

(a) Experiment results
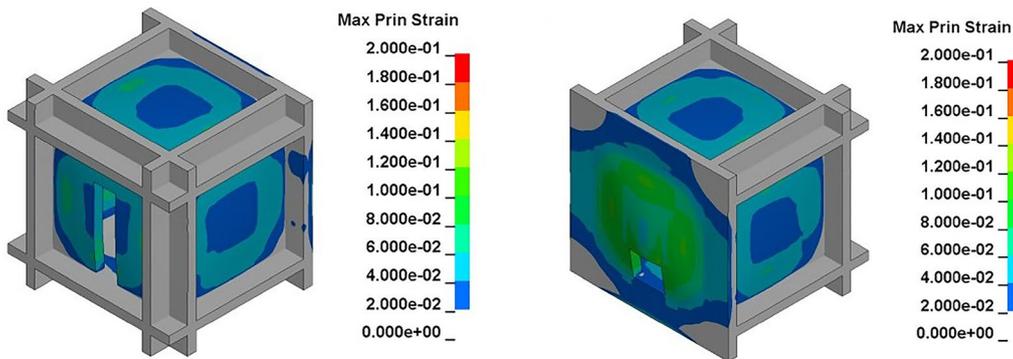
(b) Numerical simulation results without afterburn
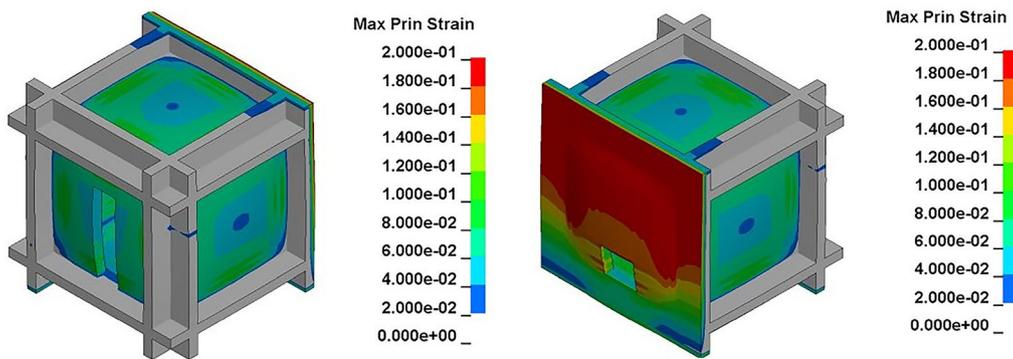
(c) Numerical simulation results with afterburn

Fig. 23 Deformation comparison.

Kim *et al. Int J Concr Struct Mater*   *(2022) 16:6*

Page 16 of 21
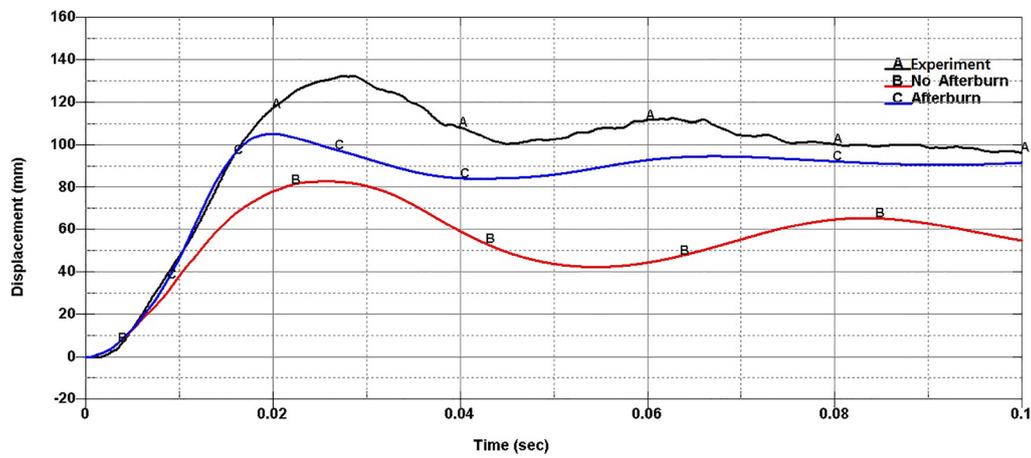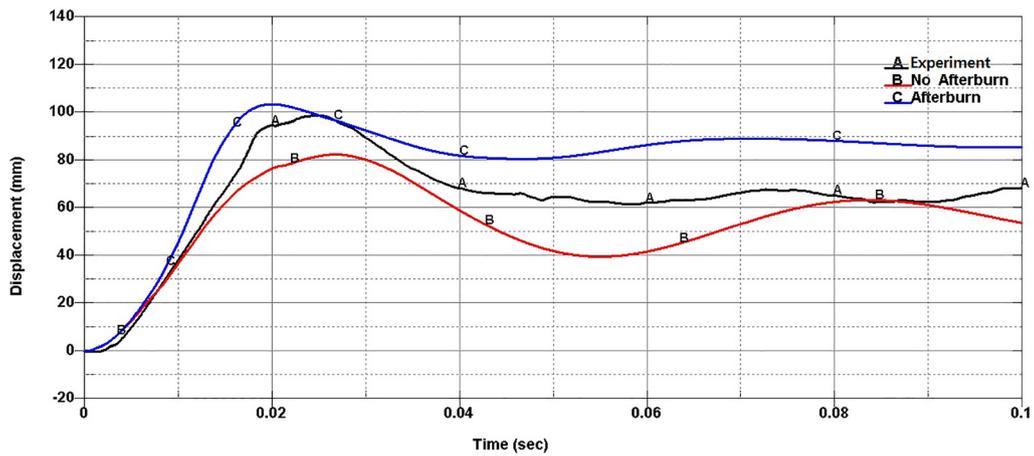

(a) Top center

(b) Right center

Fig. 24 Comparison of displacement over time.

Table 4 Displacement comparison.

| Position		Maximum (mm)	Error (%)	Final (mm)	Error (%)
Experiment	Top center	132.6	–	96.4	–
	Right center	98.8	–	68.3	–
No Afterburn	Top center	82.9	− 35.0	57.3	− 31.9
	Right center	82.5	− 21.1	53.8	− 22.8
Afterburn	Top center	105.5	− 17.3	91.8	9.1
	Right center	103.5	− 1.0	85.4	22.5

(a) Experiment results
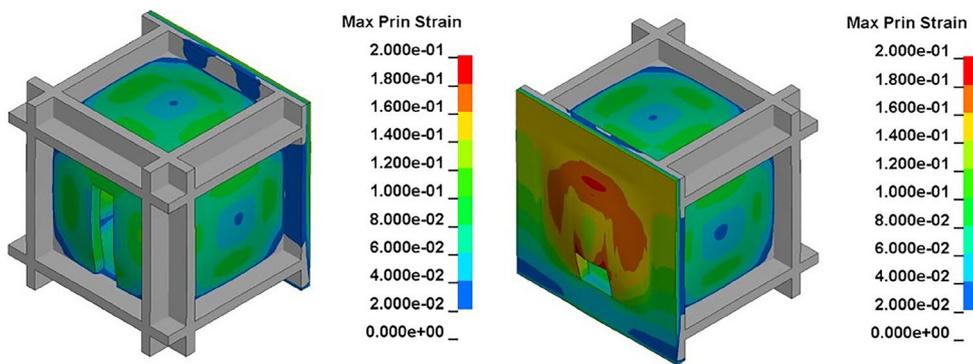
(b) Numerical simulation results without afterburn
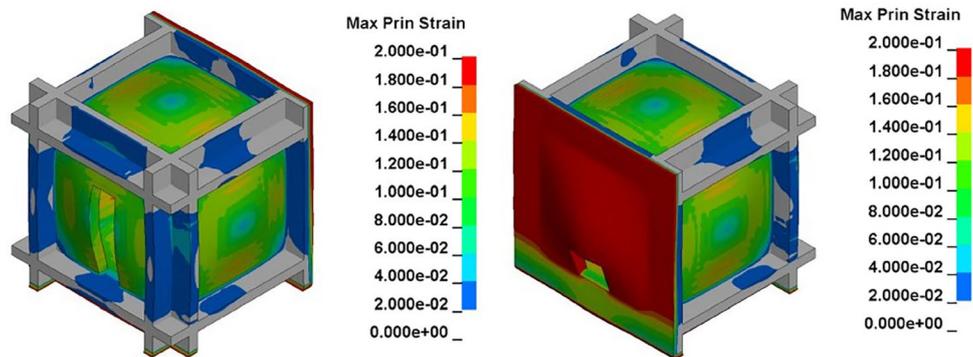
(c) Numerical simulation results with afterburn

Fig. 25 Deformation comparison.

Kim *et al. Int J Concr Struct Mater*   (2022) 16:6

Page 18 of 21
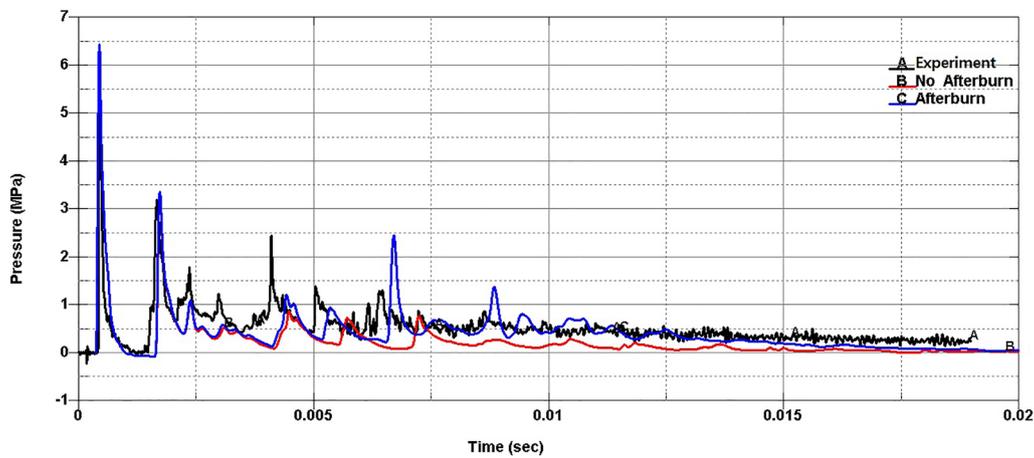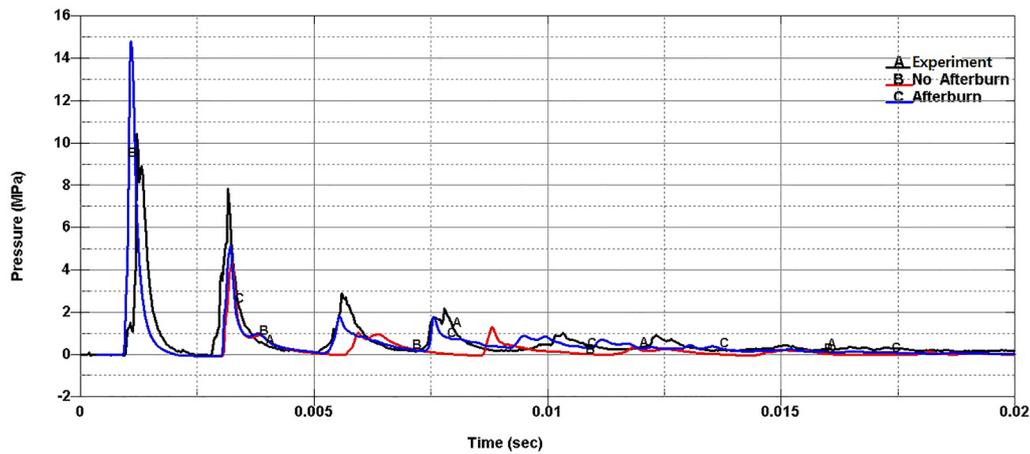
(a) Right center

(b) Right corner

Fig. 26 Pressure comparison over time.

be obtained for the 3 kg experiment. In the calculation, when afterburning was applied, the final displacement increased by 102.9% and 99.9% for both "top center" and "right center".

5 Conclusion

This study analyzed the effect of afterburning on pressure, impulse, and structural damage following an interior explosion in a Korean apartment room with two openings (a door and a window), using interior explosion experiments and numerical analyses. The research and the derived results were as follows.

Reinforced concrete rooms that mimic a scaled-down Korean-style apartment were built. Interior explosion experiments for 2 kg and 3 kg of TNT were performed to obtain data on blast pressure, impulse and displacement in the room. They were used to build a simulation model and to verify its reliability.

Using the LS-DYNA™ code, the simulation model was constructed to simulate the afterburning phenomenon. The mapping technology was built to model blast propagation precisely, and structural models and material models were constructed. Above all, the process was established to determine the afterburning energy, the afterburning start time and the end time required for the afterburning simulation model.

Numerical analyses of the effects of afterburning were performed for interior explosions of 2 kg and 3 kg of TNT using the constructed simulation model, and the results were compared with the results of simulations without afterburning, and with the results of related experiments.
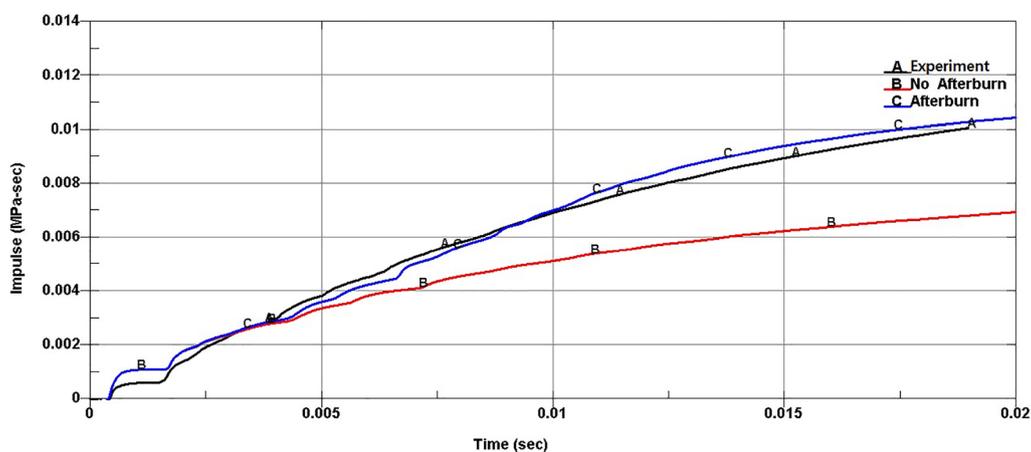
(a) Right center
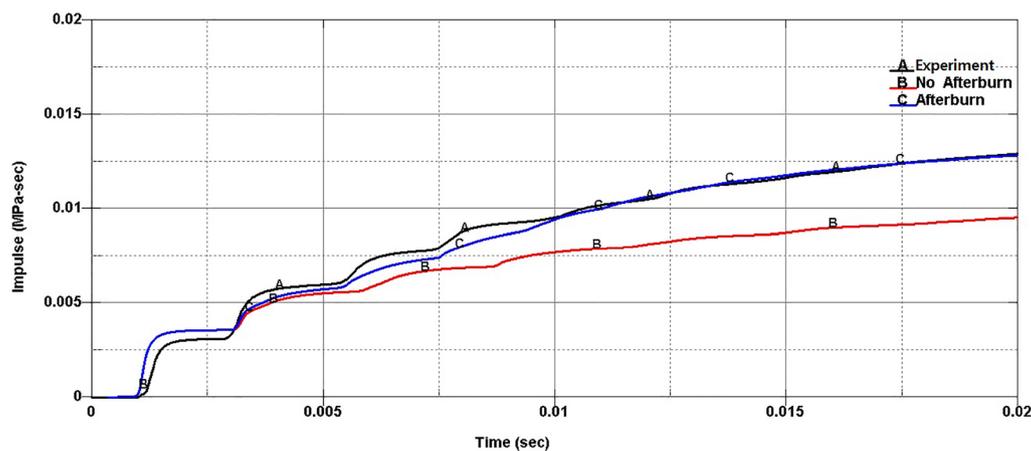
(b) Right corner

Fig. 27 Impulse comparison over time.

Table 5 Comparison of peak pressure and impulse

Position (TNT: 3 kg)		Peak pressure (MPa)						Impulse (MPa-msec)	
		1st	Error (%)	2nd	Error (%)	3rd	Error (%)	–	Error (%)
Experiment	Right center	5.419	–	3.192	–	1.786	–	10.07	–
	Right corner	10.462	–	7.840	–	2.916	–	12.91	–
No Afterburn	Right center	6.436	18.8	3.356	5.1	1.077	− 39.7	6.94	− 31.1
	Right corner	14.805	41.5	4.405	− 43.8	1.037	− 64.4	9.53	− 26.2
Afterburn	Right center	6.436	18.8	3.370	5.6	1.212	− 32.1	10.44	3.7
	Right corner	14.801	41.5	5.140	− 34.4	1.837	− 37.0	12.83	− 0.6

The numerical simulation results, which included the effects of afterburning, were generally in good agreement with the experimental results. This analysis confirmed the reliability of the simulation model. In addition, it was determined that for an interior explosion, afterburning had a large effect on the wall fracture behavior.

Kim *et al. Int J Concr Struct Mater*   (2022) 16:6

Page 20 of 21
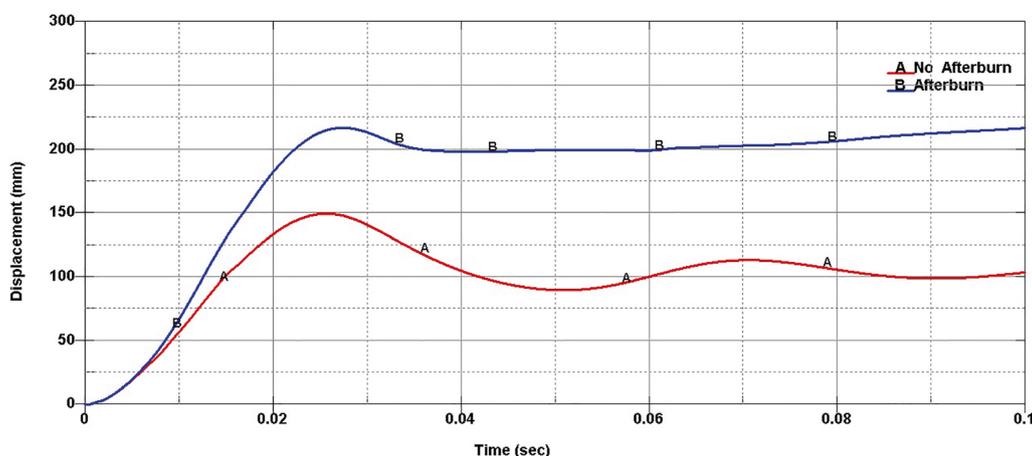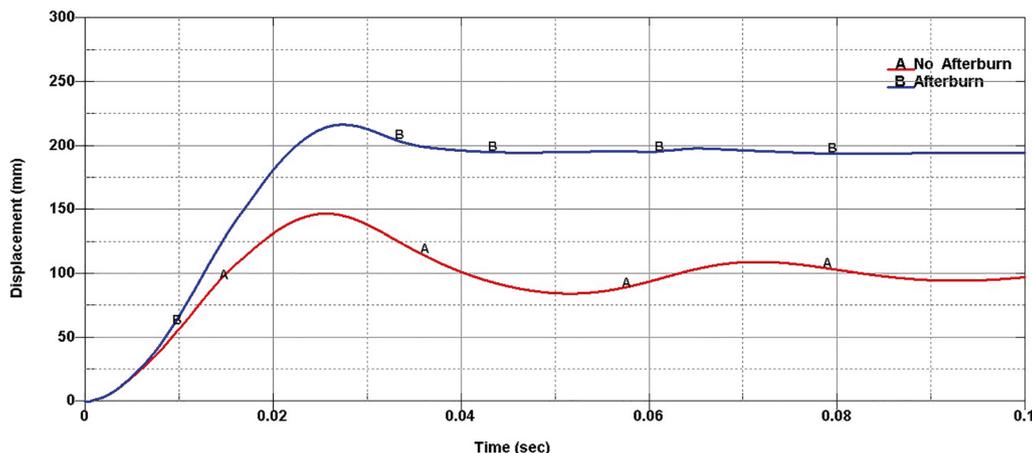
(a) Right center

(b) Right bottom

Fig. 28 Comparison of displacement over time.

Table 6 Displacement comparison.

Position		Maximum (mm)	Final (mm)
No Afterburn	Top center	149.5	103.6
	Right center	146.9	97.4
Afterburn	Top center	217.0	210.2
	Right center	216.7	194.7

The results show that the established numerical simulation model can be used for various simulation analyses of interior explosions, and will be further refined in the future.

Authors' contributions
HJK planed this paper, supervised the experiments, constructed the numerical simulation model, and analyzed the experiment results and the simulation results. KH constructed the numerical simulation model, and analyzed the experiment results and the simulation results. YHY constructed the numerical simulation model, conducted the numerical simulations, and analyzed the simulation results. HJL constructed the numerical simulation model, conducted the numerical simulations, and analyzed the simulation results. All authors read and approved the final manuscript.

Authors' information
HJK: Principal Researcher, Agency for Defense Development. KH: Ph.D, Principal Researcher, Agency for Defense Development. YHY: Principal Research Engineer, Korea Simulation Technologies Co., Ltd. HJL: Junior Research Engineer, Korea Simulation Technologies Co., Ltd.

Kim *et al. Int J Concr Struct Mater*   (2022) 16:6

Page 21 of 21

Availability of data and materials
All data generated or analysed during this study are included in this published article [and its additional information files].

Declarations

Competing interests
The authors declare that they have no competing interests.

Author details
[1]Agency for Defense Development, Daejeon, Republic of Korea. [2]Korea Simulation Technologies Co., Ltd., Gyeonggi-do, Republic of Korea.

References
Beppu, M., Ohno, T., Ohkubo, K., Li, B., & Satoh, K. (2010). Contact explosion resistance of concrete plates externally strengthened with FRP Laminates. *International Journal of Protective Structures, 1*(2), 257–270.

Cao, W., He, Z., & Chen, W. (2014). Experimental study and numerical sumulation of the afterburning of TNT by underwater explosion method. *Shock Waves, 24*, 619–624.

Edri, I., Feldgun, V. R., Karinski, Y. S., & Yankelevsky, D. Z. (2012). On blast pressure analysis due to a partially confined explosion: III. Afterburning Effect. *International Journal of Protective Structures, 3*, 311–331.

Esteban, B., & Gebbeken, N. (2016). A comparison of numerical modelling strategies in contact detonation scenarios with concrete targets. *International Journal of Computational Methods Experimantal Measures, 4*(3), 231–246.

Li, B., Nair, A., & Kai, Q. (2012). Residual axial capacity of reinforced concrete columns with simulated blast damage. *Journal of Performance of Constructed Facilities, ASCE, 26*, 287–299.

Li, J., & Hao, H. (2014). Numerical study of concrete spall damage to blast loads. *International Journal of Impact Engineering, 68*, 41–55.

Li, J., Wu, C., Hao, H., & Su, Y. (2015). Investigation of ultra-high performance concrete under static and blast loads. *International Journal of Protective Structures, 6*(2), 217–235.

Li, J., Wu, C., Hao, H., & Su, Y. (2017). Experimental and numerical study on steel wire mesh reinforced concrete slab under contact explosion. *Materials & Design, 116*, 77–91.

Lia, J., Chengqing, Wu., Hao, H., & Yu, Su. (2015). Investigation of ultra-high performance concrete under static and blast loads. *International Journal of Protective Structures, 6*(2), 217–235.

Luccioni, B. M., Aráoz, G. F., & Labanda, N. A. (2013). Defining Erosion Limit for Concrete. *International Journal of Protective Structures, 3*, 315–340.

Mao, L., Barnett, S., Begg, D., Schleyer, G., & Wight, G. (2014). Numerical simulation of ultra high performance fibre reinforced concrete panel subjected to blast loading. *International Journal of Impact Engineering, 64*, 91–100.

Mao, L., Barnett, S. J., Tyas, A., Warren, J., Schleyer, G., & Zaini, S. (2015). Response of small scale ultra high performance fibre reinforced concrete slabs to blast loading. *Construction and Building Materials, 93*, 822–830.

Ngo, T., Mendis, P., & Krauthammer, T. (2007). Behavior of ultrahigh-strength prestressed concrete panels subjected to blast loading. *Journal of Structural Engineering, 133*, 1582–1590.

Schwer, L. E. & Malvar L. J. (2005). Simplified Concrete Modeling with *Mat_Concrete_Damage_Rel3, Ls-Dyna User Week, Ana Hotel, Nagoya, 1–14, November, 2005.

Schwer, L.E. (2016). Jones-Wilkins-Lee(JWL) Equation of State with Afterburning. In: the 14th International LS-DYNA Users Conference, Rotal Dearbone Hotel & Convention Center, Detroit (p. 1–38).

Togashi, F., Baum, J. D., Mestreau, E., Löhner, R., & Sunshine, D. (2010). Numerical simulation of long-duration blast wave evolution in confined facilities. *Shock Waves, 20*, 409–424.

Wang, F., Wan, Y.K.M.W., Chong, Q.Y.K., Lim, C.H. (2009). Reinforced concrete slab subjected to close-in explosion. In: Proceedings of the second international workshop on performance, protection and strengthening of structures under extreme loading, Hayama, Japan.

Wu, C., Oehlers, D. J., Rebentrost, M., Leach, J., & Whittaker, A. S. (2009). Blast testing of ultra-high perfomance fibre and FRP-retrofitted concrete slabs. *Engineering Structures, 31*, 2060–2069.

Xu, K., & Lu, Y. (2006). Numerical simulation study of spallation in reinforced concrete plates subjected to blast loading. *Computers & Structures, 84*, 431–438.

Yue, S., Qiu, Y., Zhang, N., & Wang, M. (2017). Analytical study of local damage on concrete slab subjected to a contact explosion. *Journal of Vibroengineering, 19*(2), 908–929.

Zhang, F. R., Wu, C. Q., Wang, H. W., & Zhou, Y. (2015). Numerical simulation of concrete filled steel tube columns against BLAST loads. *Thin-Walled Structures, 92*, 82–92.

Zhou, X., Kuznetsov, V., Hao, H., & Waschl, J. (2008). Numerical prediction of concrete slab response to blast loading. *International Journal of Impact Engineering, 35*, 1186–1200.

Publisher's Note
Springer Nature remains neutral with regard to jurisdictional claims in published maps and institutional affiliations.